applied optics

Design of a compact hyperspectral imaging spectrometer with a freeform surface based on anastigmatism

Jialun Zhang,[1,2] Chao Lin,[1] Zhenhua Ji,[1] Hao Wu,[1,2] Chengliang Li,[1] Bowen Du,[1,2] and Yuquan Zheng[1,*]

[1]Changchun Institute of Optics, Fine Mechanics and Physics, Chinese Academy of Sciences, Changchun 130033, China
[2]University of Chinese Academy of Sciences, Beijing 100049, China
*Corresponding author: zhengyq@sklao.ac.cn

Received 11 October 2019; revised 19 December 2019; accepted 3 January 2020; posted 7 January 2020 (Doc. ID 379390); published 17 February 2020

Hyperspectral imaging spectrometers with a wide field of view (FoV) have significant application values. However, enhancing the FoV will increase the volume of the imaging spectrometer and reduce the imaging quality, so a wide-FoV spectrometer system is difficult to design. Based on the theory of off-axis astigmatism, we present a method that includes a "prism box," "partial anastigmatism," and a partial differential equation to solve the parameters of a freeform surface. In this method, a compact wide-FoV imaging spectrometer with a freeform surface is designed. The spectrometer is an Offner structure with two curved prisms as the dispersion elements. The primary mirror and tertiary mirror of the Offner spectrometer are an aspheric surface and a freeform surface, respectively, to correct the off-axis aberration of a wide FoV. The ratio of the slit length to the total length of the spectrometer is close to 0.4. In comparison to conventional spectrometers of the same specifications, the total length of the spectrometer is reduced by 40% and the volume by 70%. The compact imaging spectrometer has potential application in the field of space remote sensing. In addition, the design method of the spectrometer provides a reference for the design of other optical systems with freeform surfaces.

https://doi.org/10.1364/AO.379390

1. INTRODUCTION

Hyperspectral imaging spectrometers are used to simultaneously detect space information and spectral information, and they play an important role in the field of remote sensing [1–3]. In general, spectrometers have a smaller field of view (FoV), which results in a smaller detecting coverage. Enhancing the FoV will increase the volume of the imaging spectrometer and reduce the imaging quality, which restricts the application of the spectrometer. The development of an imaging spectrometer with a compact structure and a wide FoV has become the key to improving the detecting efficiency [4,5].

In order to solve the aforementioned problem, a freeform surface can be used in a specific position of the spectrometer. The development of testing and manufacturing technologies makes the application of a freeform surface in practical optical systems more convenient. The multi-degree of freedom of a freeform surface can significantly improve the performance of the optical system and correct the off-axis aberration of the large FoV [6–11]. At present, freeform surfaces have been widely used in imaging systems such as the structure of a three-mirror anastigmat (TMA). At the same time, the application of freeform surfaces in spectrometers has also been widely studied in recent years. Xu *et al.* used a freeform surface in a Czerny–Turner spectrometer to reduce the astigmatism [12]. Reimers *et al.* studied the role of a freeform surface in expanding the spectral range and reducing the volume of the spectrometer, which proves that the freeform surface can significantly improve the performance of the spectrometer [13]. Liu *et al.* designed and analyzed spectrometers with different structures and concluded that freeform surfaces can improve the performance of spectrometers [14]. Feng *et al.* integrated two spectrometers in the Environmental Mapping and Analysis Program (ENMAP) into one system and placed a filter in front of the image plane to split the beams. The astigmatism of the visible-near-infrared (VNIR) and shortwave-infrared (SWIR) ranges of the system are corrected by a lens and a freeform surface, respectively. The volume of the system with a freeform surface is reduced by 60% [15].

Nodal aberration theory (NAT) can describe the aberration field behavior in optical systems with freeform surfaces. If the freeform surface is in the stop or pupil, the net aberration contribution of the freeform surface would be a field constant [16]. In this paper, a freeform surface is used to compensate for the aberrations of different FoVs and different wavelengths, so the freeform surface is located at the tertiary mirror of the Offner spectrometer. We present a set of methods for designing a spectrometer with a freeform surface, which are mainly divided into two parts: the design of an ordinary structure and the liberalization of the tertiary mirror [17,18]. On this basis, we design a compact prism spectrometer. The spectrometer consists of two mirrors and two prisms; the primary mirror and tertiary mirror of the spectrometer use an aspheric surface and a freeform surface, respectively, to compensate for the serious off-axis aberration. The spectrometer has a spectral range of 400–800 nm, F-number of 5, and slit length of 70 mm, and the ratio of slit length to the system length is close to 0.4. The size of a single pixel is 13 μm × 13 μm. The modulation transfer functions (MTFs) of the spectrometer are close to the diffraction limit. Moreover, the maximum value of smiles is less than 0.24 pixels at the wavelength of 400 nm, and the maximum value of keystones is less than 2.5% pixels at the FoV of 35 mm. The freeform surface plays an important role in this spectrometer. The spectrometer designed in this paper is characterized by compactness, good performance, and large FoV.

2. DESIGN METHOD OF A FREEFORM SURFACE

A. "Prism Box" and "Partial Anastigmatism" Methods

There is no doubt that a good initial structure can significantly reduce the difficulty of optical design. Calculating the initial structure is the first step of optical design [19]. Unlike other optical structures, there are multiple optical elements in our scheme, and the light paths of refraction and reflection are complex. Therefore, it is difficult to obtain the initial structure with a freeform surface in our system, and it is a challenge to calculate the parameters of the freeform surface in an initial structure. In this paper, we propose a method that includes "prism box," "partial anastigmatism," and a partial differential equation to find the parameters of a freeform surface. Using this method, we designed an initial structure of the spectrometer with a freeform surface, and it is a good starting point for further optimization.

The schematic diagram of the prism box is shown in Fig. 1. To simplify the optical system, we regard the part before the freeform surface in the spectrometer as a whole and name it the prism box. When analyzing the aberrations of the spectrometer, we are only concerned with the output of the prism box, and the properties of the prism box can be studied separately. After that, we design the initial freeform surface. In this simplified structure, the beam that reaches the freeform surface is not the ideal beam, and it carries the aberrations produced by the prism box. The aberrations should be corrected by the freeform surface.

Astigmatism is the main aberration of an off-axis optical system, and it is often used as the main evaluation index of image quality [20]. In our scheme, astigmatism cannot be completely corrected only by a freeform surface. Therefore, we allow the beams in the initial spectrometer to have slight astigmatism at the beginning. We propose a more realistic "partial anastigmatism" method, which achieves a compromise between the image quality and the complexity of a freeform surface. The astigmatism Δx_{ts} of the system can be expressed by Eq. (1):

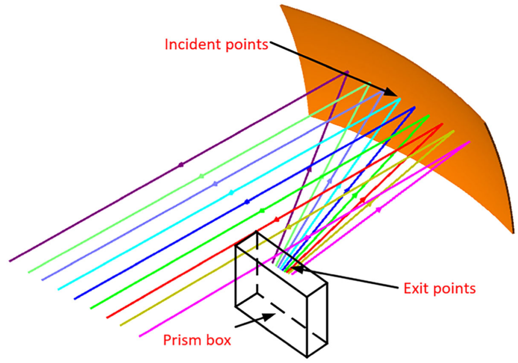

Fig. 1. Schematic diagram of the prism box.

$$\Delta x_{ts} = x_{ts-\text{prismbox}} + x_{ts-\text{freeform}}, \tag{1}$$

where $x_{ts-\text{prismbox}}$ is the astigmatic produced by the prism box and $x_{ts-\text{freeform}}$ is the astigmatic produced by the freeform surface.

B. Method for Solving the Parameters of a Freeform Surface by a Partial Differential Equation

According to the Coddington equation [21], the astigmatism Δx_{ts} of the system can be obtained by the tangential distance t' minus the sagittal distance s'. t' and s' have the relationship of $t' = \delta * s'$, where δ is a nonzero parameter determined by the ability of the freeform surface to correct astigmatism. If δ is equal to 1, the spectrometer produces no astigmatism. Otherwise, the spectrometer has astigmatism. The relationship between tangential radius r_t and sagittal radius r_s is described as follows:

$$\frac{r_t}{r_s} = \frac{\delta * t(n's - ns')}{s\,(n't\cos^2(I') - n\delta * s'\cos^2(I))}, \tag{2}$$

where t and s are tangential object distance and sagittal object distance, respectively; n and n' are the refractive indices of the object space and image space, respectively; and I and I' are the incident angle and exit angle, respectively. In this paper, a partial differential equation is used in the design process of the freeform surface in the spectrometer. Every point on the freeform surface is continuous, so the freeform surface is a regular surface. The normal vector $\vec{n}$ of the regular surface $\vec{FS}$ is

$$\vec{n} = \frac{\vec{FS_u} \times \vec{FS_v}}{|\vec{FS_u} \times \vec{FS_v}|}, \tag{3}$$

where u and v are the parameters of the regular surface, and $\vec{FS_u}$ and $\vec{FS_v}$ are the first-order partial derivatives of the regular surface.

The first and second basic expressions I and II of the regular surface are expressed by Eqs. (4) and (5), respectively:

$$\mathrm{I} = d\,\vec{FS}^2 = E(u, v)du^2 + F(u, v)dudv + G(u, v)dv^2, \tag{4}$$

$$\mathrm{II} = -d\,\vec{FS}\cdot d\,\vec{n} = L(u,v)du^2 + 2M(u,v)dudv + N(u,v)dv^2, \tag{5}$$

where E, F, G, L, M, and N are the fundamental magnitudes of the regular surface, which can be expressed by first-order and second-order partial derivatives in spherical coordinates. In order to simplify the calculation, $\vec{FS}$ is expressed by spherical coordinates as

$$\vec{FS} = \vec{FS}(\theta,\varphi), \tag{6}$$

where θ and φ are vertical and horizontal variables, respectively.

The direction vector $\vec{H}$ of the incident ray is as follows:

$$\vec{H}(\theta,\varphi) = (\cos(\theta)\cos(\varphi), \cos(\theta)\sin(\varphi), \sin(\theta)). \tag{7}$$

The incident angle I of the beam is the angle between $\vec{H}$ and $\vec{n}$, which can be obtained by Eq. (8):

$$\cos(I) = \frac{r\cos(\theta)}{\sqrt{\left(r^2 + \left(\frac{dr}{d\theta}\right)^2\right)\cos^2(\theta) + \left(\frac{dr}{d\varphi}\right)^2}}, \tag{8}$$

where r is a function of θ and φ.

The Gauss curvature K of a point in the regular surface can be expressed as the product of two principal curvature at that point, and the average curvature H can be expressed as the arithmetic square root of two principal curvatures. The characteristic equation of the principal curvature λ of the regular surface is

$$\lambda^2 - 2H\lambda + K = 0. \tag{9}$$

The Gauss curvature K and average curvature H can be calculated from the fundamental magnitudes, and the calculation equations are

$$K = \frac{LN - M^2}{EG - F^2}, \tag{10}$$

$$H = \frac{LG - 2MF + NE}{2(EG - F^2)}. \tag{11}$$

The tangential curvature ρ_t and sagittal curvature ρ_s can be expressed by the characteristic roots λ_1 and λ_2 as follows:

$$\rho_t = \lambda_1, \quad \rho_s = \lambda_2. \tag{12}$$

According to Eqs. (9–11), the characteristic roots are

$$\lambda_1 = \frac{(LG - 2MF + NE)}{2(EG - F^2)} + \frac{\sqrt{(LG - 2MF + NE)^2 - 4(LN - M^2)(EG - F^2)}}{2(EG - F^2)}, \tag{13}$$

$$\lambda_2 = \frac{(LG - 2MF + NE)}{2(EG - F^2)} - \frac{\sqrt{(LG - 2MF + NE)^2 - 4(LN - M^2)(EG - F^2)}}{2(EG - F^2)}. \tag{14}$$

According to Eqs. (12–14), the ratio of tangential curvature to sagittal curvature is

$$\frac{\rho_t}{\rho_s} = \frac{(LG - 2MF + NE) + \sqrt{(LG - 2MF + NE)^2 - 4(LN - M^2)(EG - F^2)}}{(LG - 2MF + NE) - \sqrt{(LG - 2MF + NE)^2 - 4(LN - M^2)(EG - F^2)}}. \tag{15}$$

Meanwhile, from Eqs. (8) and (2), the ratio of tangential curvature to sagittal curvature can also be expressed as follows:

$$\frac{\rho_t}{\rho_s} = \frac{1}{\delta * t(n's - ns')} \times \left(s \left(n't \frac{r^2\cos^2(\theta)}{r^2\cos^2(\theta) + \left(\frac{dr}{d\theta}\right)^2\cos^2(\theta) + \left(\frac{dr}{d\varphi}\right)^2} - n\delta * s' \frac{r^2\cos^2(\theta)}{r^2\cos^2(\theta) + \left(\frac{dr}{d\theta}\right)^2\cos^2(\theta) + \left(\frac{dr}{d\varphi}\right)^2} \right) \right). \tag{16}$$

The partial differential equation based on partial anastigmatism can be obtained by combining Eqs. (15) and (16).

As shown in Fig. 2, the parameters of Q_{21} and Q_{12} can be represented by the parameters of Q_{11}, such as $\theta_{21} = \theta_{11} + \theta_{\text{variable}}$, $\varphi_{21} = \varphi_{11}$, $\theta_{12} = \theta_{11}$, $\varphi_{12} = \varphi_{11} + \varphi_{\text{variable}}$, where θ_{11}, θ_{21}, θ_{12}, φ_{11}, φ_{21}, and φ_{12} are the vertical and horizontal variables of Q_{11}, Q_{21}, and Q_{12}, θ_{variable}, and $\varphi_{\text{variable}}$ are the vertical and horizontal variables between the adjacent points. With the method proposed above, we could calculate the point coordinates on the freeform surface by solving the partial differential equation. We could obtain the shape of the freeform surface by substituting the point coordinates into the formula of freeform surfaces. Then the initial structure of the spectrometer with a freeform surface can be obtained. The optimization function is set up to optimize the coefficients to meet other aberration-correction requirements. The design process of the spectrometer is shown in Fig. 3. It should be highlighted that the

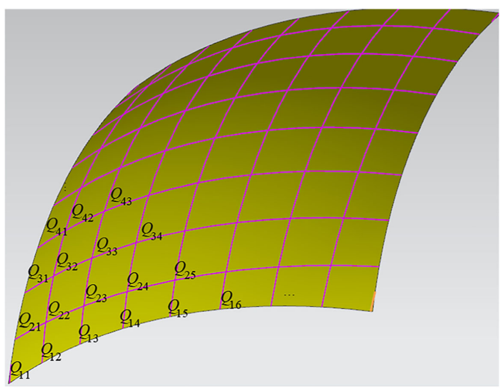

Fig. 2. Schematic diagram of calculating point coordinates of the freeform surface.

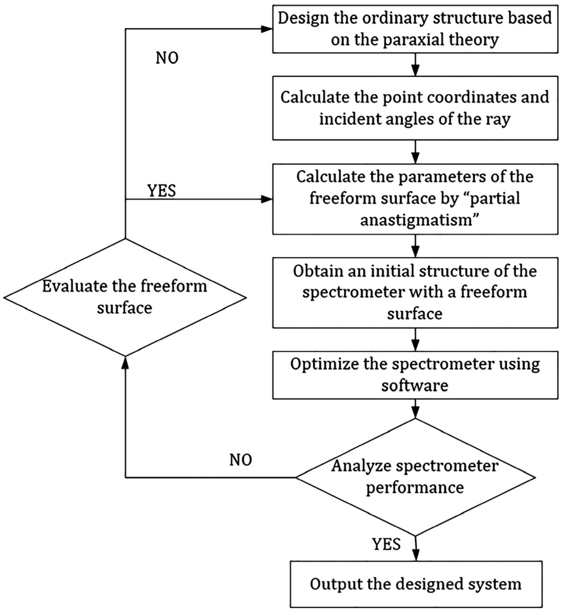

Fig. 3. Design flow of the spectrometer with a freeform surface.

ability of a freeform surface to correct aberrations is not infinite, and the requirements of the spectrometer should be reasonable.

3. DESIGN THE IMAGING SPECTROMETER

A. Overall Structure of the Imaging Spectrometer

In general, the imaging spectrometer consists of a telescope and a spectrometer. The structure of the imaging spectrometer designed in this paper is shown in Fig. 4. The object is imaged on the focal plane by a telescope. The focal plane of the telescope is the object plane of the spectrometer. The image is split by the spectrometer and focused on the detector in the form of different spectra. The imaging spectrometer obtains the spectral information of the target by the "push-broom" method.

The image plane of the telescope is also the field stop of the spectrometer. Due to the restriction of the spectroscopic principle, the spectrometer has the FoV in the form of a slit, which requires the FoV of the telescope to be a narrow rectangle. The spatial dimension X is the main direction of the FoV of the system. The spectral dimension Y is related to the detector size and other parameters. Since the TMA structure has a long focal length, a larger FoV, and no chromatic aberration, we choose the TMA structure as the front telescope of the imaging spectrometer. Through the optimization of the TMA, the pupil matching between the telescope and the spectrometer can be easily realized, and then the splicing of the imaging spectrometer can be completed.

The spectrometer is responsible for splitting the beam received by the telescope into different spectra and focusing it on the detector. The paraxial aberration theory and the Rowland circle principle show that Offner spectrometers have smaller aberration and volume. Therefore, we choose a spectrometer with an Offner structure as the spectroscopic device. Compared with gratings, prisms have higher transmittance and wider spectral range, and they are easier to manufacture. The curved prism consists of two curved spherical surfaces as shown in Fig. 5.

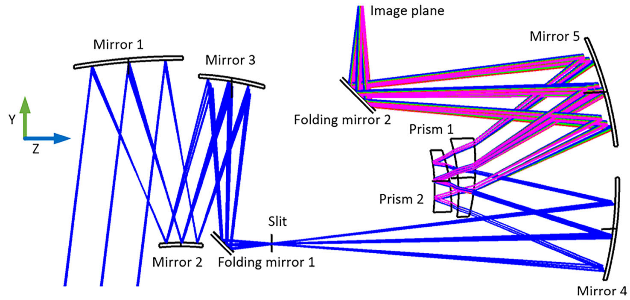

Fig. 4. Structure of the imaging spectrometer.

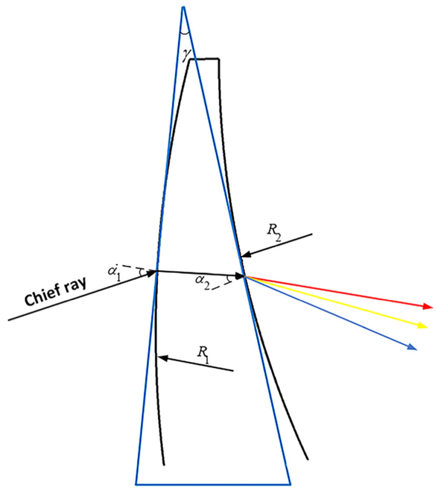

Fig. 5. Geometry diagram of the curved prism.

Based on the third-order aberration theory, the parameters of the curved prism can be calculated [22]. In addition, there is a major problem with prisms: the prism dispersion is nonlinear [23]. In the VNIR range, the phenomenon of nonlinear dispersion is very obvious. We choose crown glass and flint glass to reduce the nonlinear dispersion of the curved prisms. The curved prisms have both collimation and dispersion functions, and we use two curved prisms to split the light.

As shown in Fig. 4, the beams pass through prisms 1 and 2 twice to increase the dispersive power. The left surface of prism 2 needs to be coated with a film of high reflectivity. In the imaging spectrometer, the beam is imaged once through the TMA and then enters the Offner spectrometer. After the beam is split in the spectrometer, it is focused on the detector. The specifications of the imaging spectrometer are shown in Table 1.

B. Telescope

The FoV of the telescope is rectangular, which includes a spatial dimension and a spectral dimension. Since the spectral dimension should meet the requirements of the sampling theorem, the width of the slit should be appropriately increased, that is, the FoV of the spectral dimension of the telescope should be increased. The relationships between the focal length and FoVs of the telescope are as follows:

$$f_t' * \tan(\text{field}_x) = x_{\text{length}}, \tag{17}$$

Table 1. Specifications of the Imaging Spectrometer

Parameters	Value	Units
Spectral range	400–800	nm
Numerical aperture	0.1	—
Slit length	70	mm
Focal length	200	mm
Detector pixel size	13 × 13	μm
Spectral resolution	2.6	nm
Spectrometer length	≤ 190	mm
Spectral channel	≥ 154	—

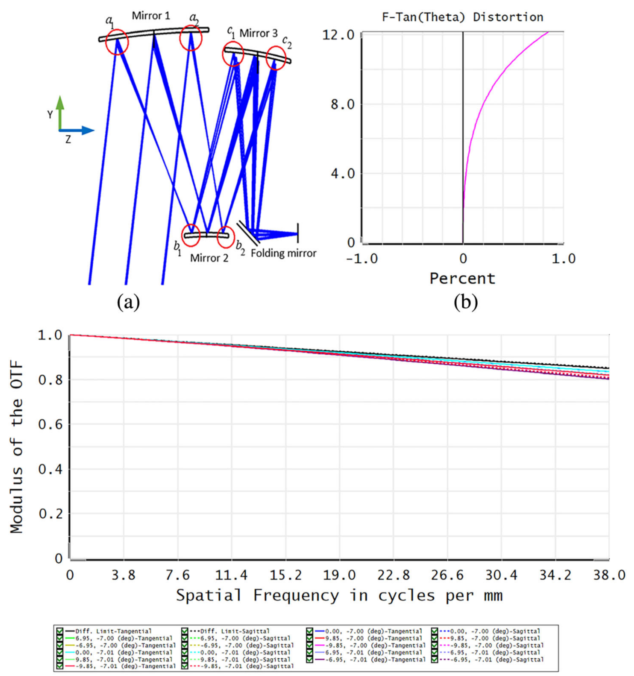

Fig. 6. Telescope: (a) optical system, (b) distortion of the telescope, (c) MTF of the telescope.

$$f_t' * \tan(\text{field}_y) = y_{\text{length}}, \quad \textbf{(18)}$$

where x_{length}, y_{length} are the length and width of the slit, respectively; field_x and field_y are the FoVs in the X and Y directions, respectively; and f_t' is the focal length of the telescope. Substituting the specifications of the detection system into Eqs. (17) and (18), the full FoV in the X direction is 19.85°. The width of the slit is set close to 4 pixels, so the full FoV in the Y direction is 0.014°.

The structure of the telescope is shown in Fig. 6(a). In the optimization, we control the edge points, such as a_1, a_2, b_1, b_2, c_1, c_2, and the tilt angles and aspheric coefficients of the three mirrors to obtain the best TMA. The FoV in the Y direction of the telescope is very small, and we focus on optimizing the X FoV. The distortion and MTF of the telescopic system are shown in Figs. 6(b) and 6(c), respectively. The maximum distortion is less than 1%. The pixel size of the detector is 13 μm, and the Nyquist frequency is 38 lp/mm, where the MTF of the telescope can reach more than 0.8.

C. Spectrometer System with a Freeform Surface

In order to simplify the design process of spectrometer, we divide the design process into two parts: 1) The spectrometer consisting of ordinary optical elements is designed by the theory of paraxial aberration. 2) The surface shape of the tertiary mirror is changed to a freeform surface by the nodal aberration theory, and the parameters of the freeform surface are determined by the prism box and partial anastigmatism methods.

In the first part of the design process, we control the length of the spectrometer system and ignore the aberrations. Then we calculate the astigmatism generated by the optical elements in front of the tertiary mirror, ie, the astigmatism of the prism box. As shown in Fig. 7, this paper presents a method for calculating the astigmatism of the prism box based on the Coddington equation. We take the ray of the marginal FoV as an example and set up a Cartesian coordinate system above the slit. The X axis and Y axis of the coordinate system are parallel to the length and width directions of the slit, respectively, and the Z axis is the direction of the ray. The centers of all optical elements of the spectrometer are on the YOZ plane. In Fig. 7, $A_i(x_i, y_i, z_i)$ is the intersection of the ray and the ith surface. $A_0(x_0, y_0, z_0)$ is the intersection of the ray and the slit, which can be considered the emission point of the ray. $A_1(x_1, y_1, z_1)$ is the intersection of the ray and primary mirror, and $A_2(x_2, y_2, z_2)$ is the first intersection of the ray and the prism surface. $O_1(x_{o1}, y_{o1}, z_{o1})$ and R_1 are the spherical center and radius of the sphere where the primary mirror is located, respectively. The space equations of the ray and primary mirror are expressed in Eqs. (19) and (20):

$$x = x_0, \quad y = y_0, \quad \textbf{(19)}$$

$$(x - x_{o1})^2 + (y - y_{o1})^2 + (z - z_{o1})^2 = R_1^2. \quad \textbf{(20)}$$

The coordinate of A_1 can be solved by Eqs. (19) and (20). The incident angle I_1 is the angle between $\overrightarrow{A_0A_1}(x_1 - x_0, y_1 - y_0, z_1 - z_0)$ and $\overrightarrow{O_1A_1}(x_1 - x_{o1}, y_1 - y_{o1}, z_1 - z_{o1})$, so I_1 can be expressed by Eq. (21):

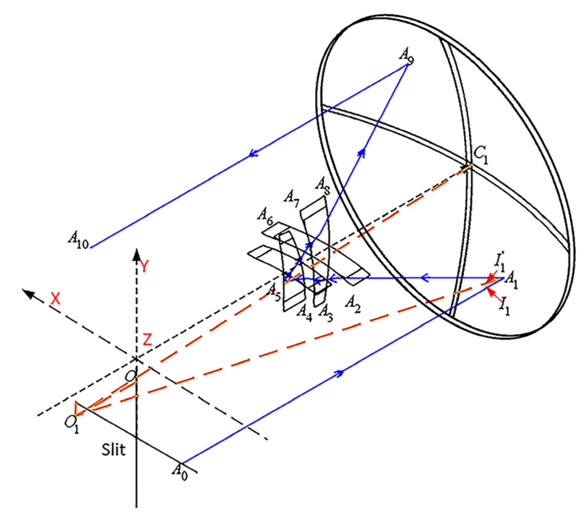

Fig. 7. Schematic diagram of the transmission of the light in the prism box.

$$I_1 = \frac{(x_1 - x_0) * (x_1 - x_{o1}) + (y_1 - y_0) * (y_1 - y_{o1}) + (z_1 - z_0) * (z_1 - z_{o1})}{\sqrt{(x_1 - x_0)^2 + (y_1 - y_0)^2 + (z_1 - z_0)^2} * \sqrt{(x_1 - x_{o1})^2 + (y_1 - y_{o1})^2 + (z_1 - z_{o1})^2}}. \quad (21)$$

When the beam just exits the slit, the tangential object distance t is equal to the sagittal object distance s. The tangential radius r_t is the same as the sagittal radius r_s since the shape of the optical elements is spherical. The refractive indices of the object side and image side of the reflection system are equal, so we can get $I = I'$ from Eq. (22) according to the Snell Principle:

$$I_1' = \frac{(x_1 - x_2) * (x_1 - x_{o1}) + (y_1 - y_2) * (y_1 - y_{o1}) + (z_1 - z_2) * (z_1 - z_{o1})}{\sqrt{(x_1 - x_2)^2 + (y_1 - y_2)^2 + (z_1 - z_2)^2} * \sqrt{(x_1 - x_{o1})^2 + (y_1 - y_{o1})^2 + (z_1 - z_{o1})^2}}. \quad (28)$$

$$I' = \arcsin\left(\frac{n \sin(I)}{n'}\right). \quad (22)$$

According to Coddington equation, after passing through the primary mirror, the tangential and sagittal image distances of the beam have the following relationships shown by Eqs. (23) and (24):

$$\frac{n'}{t'} - \frac{n}{t} = \frac{n' - n}{r_t \cos(I)}, \quad (23)$$

$$\frac{n'}{s'} - \frac{n}{s} = \frac{(n' - n)\cos(I)}{r_s}. \quad (24)$$

We also need to solve the coordinate of A_2 by spatial geometry. $O_2(x_{o2}, y_{o2}, z_{o2})$ and R_2 are the spherical center and radius of the sphere where the right surface of the right prism is located, respectively. The plane equation in space can be expressed by Eq. (25):

$$Ax + By + Cz = D, \quad (25)$$

where, A, B, C, and D are the coefficients of the plane equation. The plane $O_1A_0A_1A_2$ is determined by the coordinates of the three points O_1, A_0, and A_1. We assume the parameters x_2, y_2, and z_2 are known. The coordinate of A_2 can be solved by three equations established by three constraints, which are as follows:

(1) A_2 is a point on the surface $O_1A_0A_1A_2$;
(2) A_2 is a point on the sphere centered on O_2;
(3) I_1' is the angle between the vectors $\overrightarrow{A_2A_1}$ and $\overrightarrow{A_1O_1}$.

From the three constraints above, the three equations [Eqs. (26)–(28)] can be listed, and then the coordinates of A_2 can be obtained. The other intersection coordinates can also be calculated by the above processes. The astigmatism of the prism box can be obtained by substituting the intersection coordinates into Eqs. (23) and (24), and then the point coordinates on the freeform surface can be obtained by the method described in Section 2. The three equations are

$$Ax_2 + By_2 + Cz_2 = D, \quad (26)$$

$$(x - x_{o2})^2 + (y - y_{o2})^2 + (z - z_{o2})^2 = R_2^2, \quad (27)$$

Freeform surfaces are a category of nonrotational symmetric surfaces that can be expressed by many kinds of expressions, such as NURBS, XY, and Zernike polynomials. In these freeform surfaces, XY polynomials were the first type of polynomials used for low-order freeform surfaces historically, and they still remain a common surface description of freeform surfaces. In addition, the XY polynomial surface is more convenient to establish [24–27]. Depending on a lot of design experience, the shape of the tertiary mirror domain can be determined. In conclusion, the XY polynomial surface is selected as the mirror freeform type in this paper. The direction of the slit follows the X axis. The spectrometer is symmetric about the YOZ plane, so the odd powers coefficients of x in the polynomial are zeros, and the expression of the polynomial is

$$Z = \frac{cr^2}{1 + \sqrt{1 - (1+k)c^2r^2}} + a_0x^0y^1 + a_1x^2y^0 + a_2x^0y^2 + a_3x^2y^1 + a_4x^0y^3 + a_5x^4y^0 + a_6x^2y^2 + a_7x^0y^4 + \cdots, \quad (29)$$

where c is the curvature, r is the radius, and k is the quadratic coefficient. The freeform surface can be fitted from point coordinates. The surface shape is shown in Fig. 8, which is expressed by the fourth-order XY polynomial. The polynomial coefficients of the freeform surface are shown in Table 2.

Figure 9 shows the MTFs of the spectrometer before and after adding a freeform surface. The MTF of the spectrometer is increased by more than 30% after adding a freeform surface, which satisfies the purpose of correcting partial astigmatism. In our design, the freeform surface is placed at the position of the

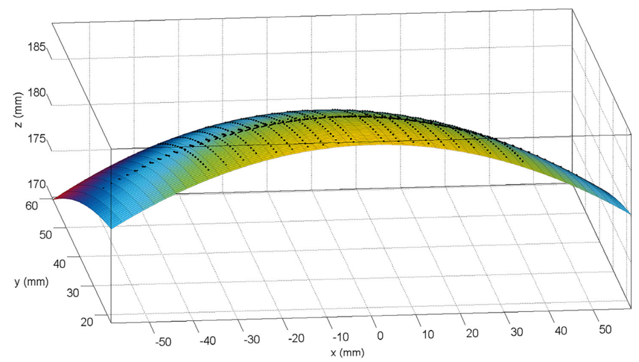

Fig. 8. Freeform surface fitted by XY polynomial.

Table 2. XY Polynomial Coefficient

Item	Coefficient a_i	Item	Coefficient a_i
x^0y^1	0.02159	x^0y^3	0.02379
x^2y^0	0.00239	x^4y^0	0.09489
x^0y^2	0.00089	x^2y^2	0.25228
x^2y^1	0.46045	x^0y^4	0.11529

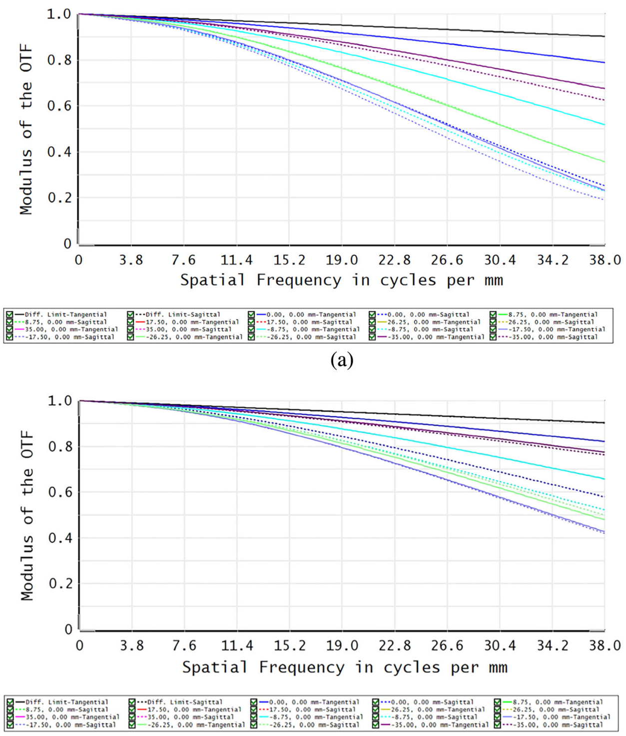

Fig. 9. MTFs of spectrometer: (a) MTF without a freeform surface and (b) MTF with a freeform surface.

tertiary mirror to correct the off-axis aberrations. Since the volume of the spectrometer is small and the length ratio of the slit to the spectrometer is close to 0.4, the aberration of the system is relatively large. A freeform surface cannot compensate for all the aberrations of the system. Therefore, we set the primary mirror to be aspheric and increased the coefficients of the freeform surface to the fifth order. The structure of the spectrometer is shown in Fig. 10, the basic parameters of the spectrometer are shown in Table 3, and the coefficients of aspheric surface and freeform surface are shown in Tables 4 and 5, respectively.

4. PERFORMANCE ANALYSIS OF THE IMAGING SPECTROMETER

The aberration correction ability of the spherical elements is limited. If spherical elements have been used to achieve the designed specifications, the length of the spectrometer is 340 mm and the overall size is 340 mm × 192 mm × 148 mm. The spectrometer that we designed has a length of 190 mm and an overall size of 190 mm × 118 mm × 107 mm. The length of the spectrometer is reduced by more than 40% and the volume by more than 70%.

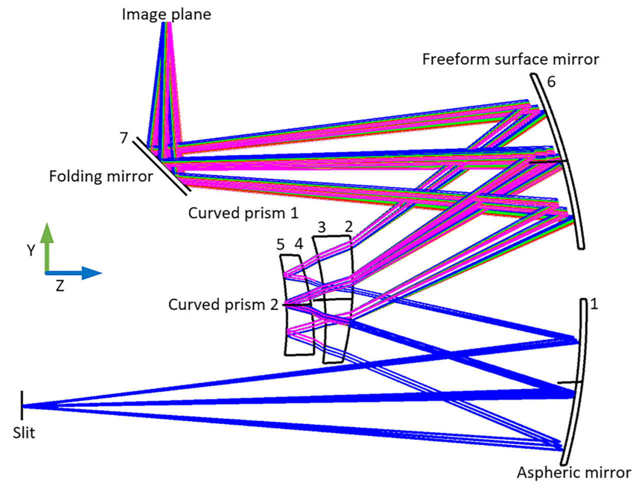

Fig. 10. Structure of the spectrometer.

Table 3. Basic Parameters of the Spectrometer

Surface	Surface Type	Radius (mm)	Thickness (mm)	Material	Tilt Angle (degree)
1	Aspherical mirror	−198.1	77.1	Mirror	2.4
2	Spherical	113.8	−10	SF4	1.3
3	Spherical	100.8	5.2	—	7.1
4	Spherical	96.5	7.6	SILICA	−12
5	Spherical	102.5	7.6	Mirror	6.1
10	XY polyn-omial	−198	−190	Mirror	2.6

Table 4. Aspheric Coefficients of the Primary Mirror

Item	Fourth Order	Sixth Order	Eighth Order
Coefficient	6.0072e-009	7.3663e-014	1.7558e-019

Table 5. Freeform Surface Coefficients of the Tertiary Mirror

Item	Coefficient a_i	Item	Coefficient a_i	Item	Coefficient a_i
x^0y^1	0.307549	x^0y^3	0.253812	x^4y^1	0.137157
x^2y^0	0.055817	x^4y^0	0.187594	x^2y^3	0.686601
x^0y	0.060758	x^2y^2	0.987914	x^0y^5	0.195894
x^2y^1	0.120995	x^0y^4	0.074233	—	—

MTFs of different spectra of the whole system spliced by telescope and spectrometer are shown in Figs. 11(a)–11(c). All MTFs at Nyquist frequency are higher than 0.57. The spot diagrams of the system are shown in Figs. 12(a)–12(c), and all the RMS radii are smaller than the size of a single pixel.

Spectral smile and keystone are the forms of spectrometers' distortion in different FoVs and different spectra. As shown in Fig. 13, the angle between the tangent planes of the front and rear surfaces of the prism changes as the beam position

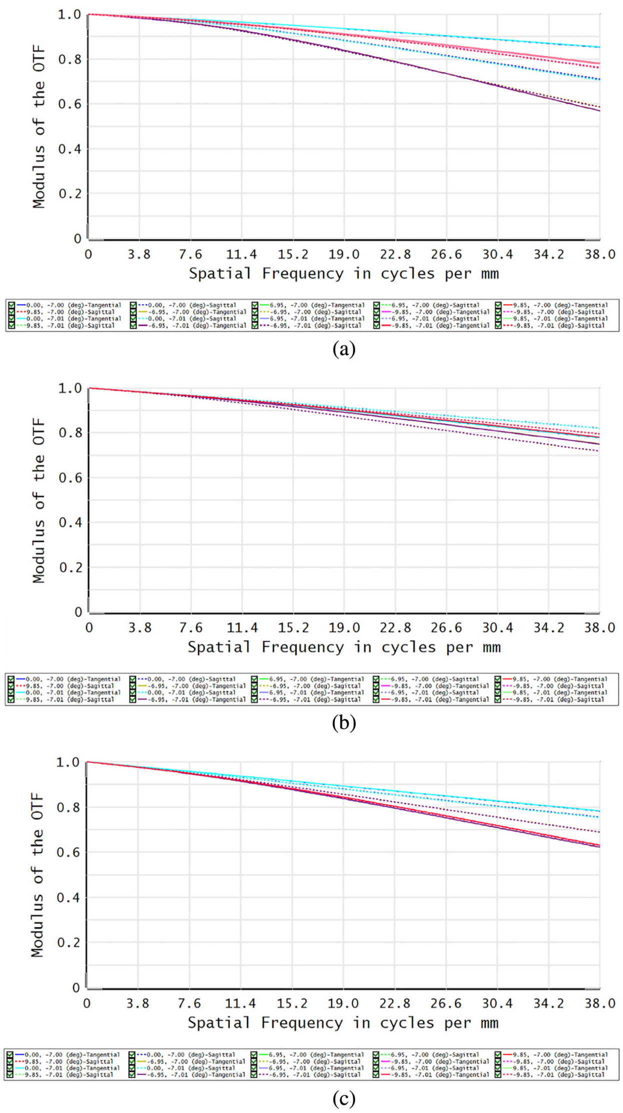

Fig. 11. MTFs of different spectra of the imaging spectrometer: (a) 400 nm, (b) 600 nm, and (c) 800 nm.

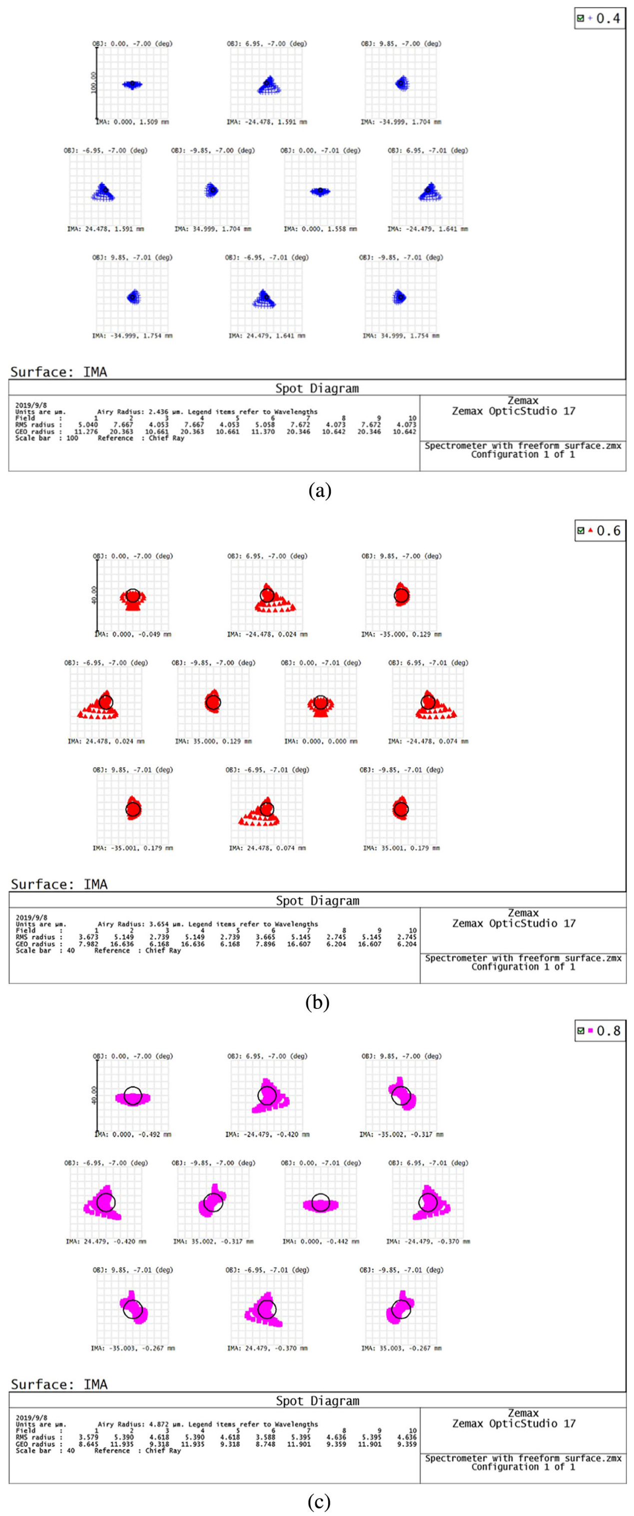

Fig. 12. Spot diagrams of different spectra of the imaging spectrometer: (a) 400 nm, (b) 600 nm, and (c) 800 nm.

changes. If the FoV has increased, the angle will increase sharply, which causes serious spectral smile. In the early optimization, we reduced the spectral smile by optimizing the curvature and tilt of the optical elements, but the effect was not ideal. As shown in Fig. 14, we designed a curved slit to correct the spectral smile. The spectral smile and keystone after using a curved slit are shown in Fig. 15(a) and Fig. 15(b), respectively. At the wavelength of 400 nm, the maximum spectral smile is less than 0.24 pixels. At 35 mm FoV, the maximum keystone is less than 2.5% pixels. The spectral resolution of the spectrometer is shown in Fig. 16; the average spectral resolution is 2.58 nm, and the result meets our requirements for the spectrometer.

5. DESIGN PRINCIPLE OF FREEFORM SURFACES

The freeform surface is an important part of the spectrometer we designed. With the development of testing and machining techniques, some complex freeform surfaces can also be manufactured. However, complex freeform surfaces result in higher costs and longer manufacturing cycles. The design principle of optical systems with freeform surfaces is to reduce the manufacturing complexity while satisfying the design specifications. Considering the actual processing needs and some existing

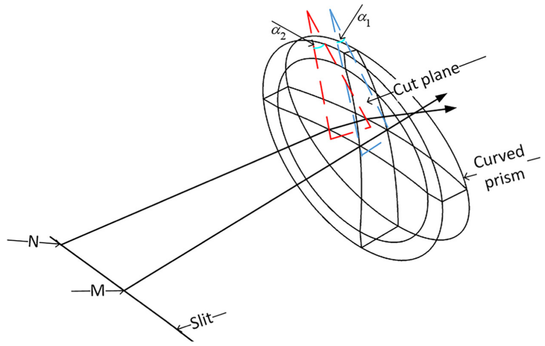

Fig. 13. Schematic diagram of the effect of a curved prism on the beam.

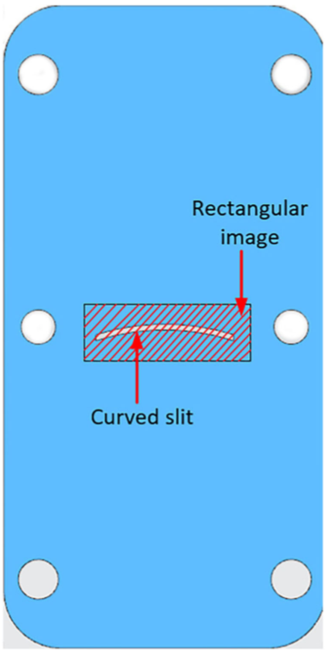

Fig. 14. Schematic diagram of a curved slit.

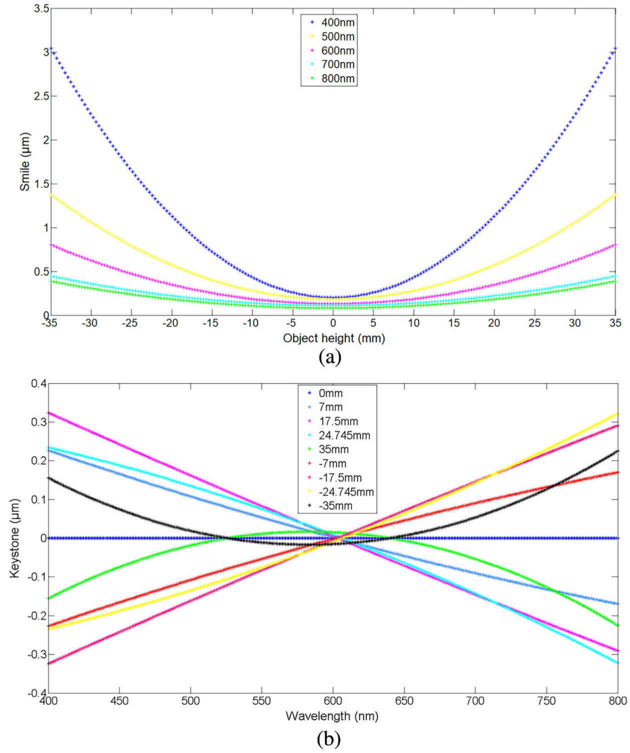

Fig. 15. (a) Spectral smile of different wavelengths and (b) keystone of different FoVs.

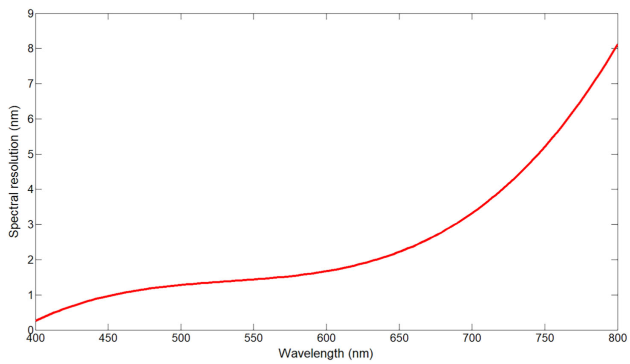

Fig. 16. Spectral resolution of different wavelengths.

processing methods, this paper controls the parameters of the freeform surface. Although this will decrease the image quality to a certain extent, the performance of the system is still within our acceptable limits.

In order to successfully complete the machining of a freeform surface, the following three principles should be considered in the design process: (1) The R# = R/D (R and D represent radius and clear diameter, respectively) of an optical element is the ratio of surface diameter to mechanical size, which represents the bending degree of the element. The larger R# is, the easier the element is to manufacture. As shown in Fig. 17, mechanical size of the tertiary mirror is very large since the light in the spectrometer is dispersed twice by the curved prisms. The tertiary mirror will converge the light onto the focal plane within a short distance, which decreases the surface diameter of the element. Therefore, the R# of a freeform surface in a spectrometer tends to be small. In order to achieve the balance between image quality and manufacturing, the R# of the freeform surface designed in this paper is 1.43. (2) A freeform surface is expressed by a polynomial. The manufacturing difficulty is related to the order of the polynomial. The accuracy of a complex freeform surface cannot be guaranteed, so a freeform surface is expressed by low-order polynomial as much as possible. (3) If there are multiple mirrors in an optical instrument, the concave mirror is usually set to a freeform surface because a concave mirror surface is easier to manufacture and test than a convex mirror surface.

Computer-generated hologram (CGH) is a highly accurate method for testing freeform surfaces [28]. In an interferometric measuring device, off-axis aspheric or freeform mirrors can be measured using a CGH as a wavefront matching element. The CGH is placed between the exit of the interferometer, and the surface under test adapts the spherical or plane wave coming from the interferometer to the surface shape of the specimen. The sag of the freeform surface designed in this paper is shown

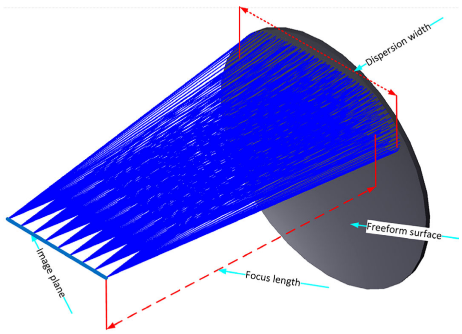

Fig. 17. Tertiary mirror focuses the beam.

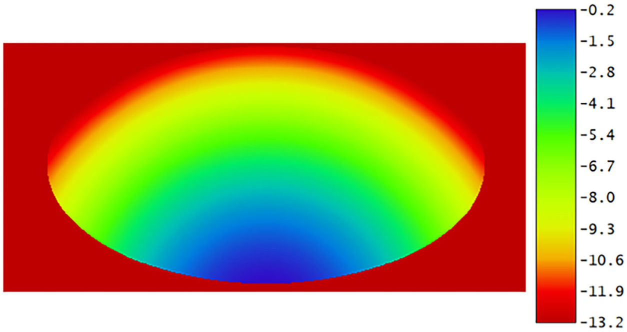

Fig. 18. Sag map of the freeform surface.

in Fig. 18. The gradient of the freeform surface changes gently, and the center deviation of the fitting sphere is small.

6. CONCLUSION

In this study, a method for designing a wide-FoV spectrometer with a freeform surface is presented. In this method, we designed a compact spectrometer. Compared with a conventional spectrometer, the length of the system based on the freeform surface is reduced by 40% and the volume by 70%. The design process of the spectrometer is divided into two parts: designing the ordinary structure and changing the shape of the tertiary mirror from a spherical surface to a freeform surface. The parameters of a freeform surface are determined by the prism box, partial anastigmatism, and partial differential equation methods. The spectrometer with a freeform surface has a compact and lightweight structure, which is helpful for the fields of aeronautics and astronautics. The design method of this paper provides a reference for the design of complex systems with freeform surfaces.

Funding. National Basic Research Program of China (973 Program) (2016YFB0500300).

Disclosures. The authors declare that there are no conflicts of interest related to this paper. We declare that we do not have any commercial or associative interests that represent a conflict of interest in connection with the work submitted.

REFERENCES

1. P. Mouroulis, R. O. Green, and T. G. Chien, "Design of pushbroom imaging spectrometers for optimum recovery of spectroscopic and spatial information," Appl. Opt. **39**, 2210–2220 (2000).
2. P. R. Silverglate, K. L. Shu, D. Perston, J. T. Stein, and F. R. Sileo, "Concepts for spaceborne hyperspectral imagery using prism spectrometers," Proc. SPIE **2267**, 112–120 (1994).
3. D. W. Warren, D. J. Gutierrez, J. L. Hall, and E. R. Keim, "Dyson spectrometers for infrared earth remote sensing," Proc. SPIE **7082**, 70820R (2008).
4. H. Qi, B. Yao, J. Wang, and L. Yuan, "The design of a wide-angle and wide spectral range pushbroom hyperspectral imager," Proc. SPIE **9263**, 92630F (2014).
5. J. Zhu, T. Yang, and G. Jin, "Design method of surface contour for a freeform lens with wide linear field-of-view," Opt. Express **21**, 26080–26092 (2013).
6. X. Zhang, L. Zheng, X. He, L. Wang, F. Zhang, S. Yu, G. Shi, B. Zhang, Q. Liu, and T. Wang, "Design and fabrication of imaging optical systems with freeform surfaces," Proc. SPIE **8486**, 848607 (2012).
7. Q. Meng, H. Wang, K. Wang, Y. Wang, Z. Ji, and D. Wang, "Off-axis three-mirror freeform telescope with a large linear field of view based on an integration mirror," Appl. Opt. **55**, 8962–8970 (2016).
8. T. Yang, J. Zhu, X. Wu, and G. Jin, "Direct design of freeform surfaces and freeform imaging systems with a point-by-point three-dimensional construction-iteration method," Opt. Express **23**, 10233–10246 (2015).
9. T. Yang, G. Jin, and J. Zhu, "Design of image-side telecentric freeform imaging systems based on a point-by-point construction-iteration process," Chin. Opt. Lett. **15**, 062202 (2017).
10. Z. Jun and H. Wei, "Design of a low F-number freeform off-axis three-mirror system with rectangular field-of-view," J. Opt. **17**, 015605 (2015).
11. T. Yang, D. Cheng, and Y. Wang, "Freeform imaging spectrometer design using a point-by-point design method," Appl. Opt. **57**, 4718–4727 (2018).
12. L. Xu, K. Chen, Q. He, and G. Jin, "Design of freeform mirrors in Czerny-Turner spectrometers to suppress astigmatism," Appl. Opt. **48**, 2871–2879 (2009).
13. J. Reimers, A. Bauer, K. P. Thompson, and J. P. Rolland, "Freeform spectrometer enabling increased compactness," Light Sci. Appl. **6**, e17026 (2017).
14. C. Liu, C. Straif, T. F. Paul, U. D. Zeitner, and H. Gross, "Comparison of hyperspectral imaging spectrometer designs and the improvement of system performance with freeform surfaces," Appl. Opt. **56**, 6894–6901 (2017).
15. L. Feng, J. Zhou, L. Wei, X. He, Y. Li, J. Jing, and B. Xiangli, "Design of a compact wide-spectrum double-channel prism imaging spectrometer with freeform surface," Appl. Opt. **57**, 9512–9522 (2018).
16. K. Fuerschbach, J. P. Rolland, and K. P. Thompson, "Theory of aberration fields for general optical systems with freeform surfaces," Opt. Express **22**, 26585–26606 (2014).
17. T. Yang, D. Cheng, and Y. Tian, "Aberration analysis for freeform surface terms overlay on general decentered and tilted optical surfaces," Opt. Express **26**, 7751–7770 (2018).
18. T. Gong, G. Jin, and J. Zhu, "Point-by-point design method for mixed-surface-type off-axis reflective imaging systems with spherical, aspheric, and freeform surfaces," Opt. Express **25**, 10663–10676 (2017).
19. Z. Zheng, X. Liu, H. Li, and L. Xu, "Design and fabrication of an off-axis see-through head-mounted display with an x-y polynomial surface," Appl. Opt. **49**, 3661–3668 (2010).
20. S. Masui, "Geometric aberration theory of double-element optical systems," J. Opt. Soc. Am. A **16**, 2253–2268 (1999).
21. Z. Malacara-Hernandez, D. Malacara-Hernandez, and A. Gómez-Vieyra, "A new derivation of a general Coddington equation from the sagittal and tangential Coddington equations," Optik **124**, 4627–4628 (2013).
22. P. F. Morrissey, "Third-order aberrations of a prism with spherically curved surfaces," Appl. Opt. **33**, 2539–2543 (1994).

23. E. Cojocaru, "Analytic expressions for the fourth- and the fifth-order dispersions of crossed prisms pairs," Appl. Opt. **42**, 6910–6914 (2003).
24. D. Cheng, Y. Wang, and H. Hua, "Free form optical system design with differential equations," Proc. SPIE **7849**, 78490Q (2010).
25. J. Y. Wang and D. E. Silva, "Wave-front interpretation with Zernike polynomials," Appl. Opt. **19**, 1510–1518 (1980).
26. I. Kaya, K. P. Thompson, and J. P. Rolland, "Comparative assessment of freeform polynomials as optical surface descriptions," Opt. Express **20**, 22683–22691 (2012).
27. G. W. Forbes, "Characterizing the shape of freeform optics," Opt. Express **20**, 2483–2499 (2012).
28. S. Scheiding, M. Beier, U. D. Zeitner, S. Risse, and A. Gebhardt, "Freeform mirror fabrication and metrology using a high performance test CGH and advanced alignment features," Proc. SPIE **8613**, 86130J (2013).